Compact and Low-Cost 3-D Printed Antennas Metalized Using Spray-Coating Technology for 5G mm-Wave Communication Systems

Shaker Alkaraki, Andre Sarker Andy, Yue Gao, Kin-Fai Tong, Zhinong Ying, Robert Donnan, and Clive Parini

***Abstract*—This letter presents a design of two compact, light, rigid, and low-cost three-dimensionally (3-D) printed millimeter-wave antennas for a fifth-generation (5G) communication system. The proposed antennas consist of a radiating slot that is surrounded by a rectangular cavity and corrugations, which boost the gain performance of the antennas. Furthermore, the proposed antennas are fabricated using 3-D printing technology, and they are metalized using novel, simple, and low-cost techniques, which utilize the commercial conducive spray-coating technology. The proposed antennas operate at a 28 GHz band, where the first design is fed by a waveguide to prove the performance, whereas the second design is fed by a microstrip line to demonstrate the ability to be integrated into a compact structure. Measurement results show a wide impedance bandwidth, which enables the proposed antenna design to be a strong candidate for 5G applications.**

***Index Terms*—Corrugations, millimeter-wave (mm-wave), slot antenna, three-dimensionally (3-D) printed antenna, 28 GHz, 5G.**

I. Introduction

THE fifth-generation (5G) mobile communications technology, which is expected to be standardized by 2020, is a promising technology, which is expected to achieve 1000 times overall system capacity, ten times data rate (i.e., peak data rate of 1 Gb/s for high mobility and 10 Gb/s for low mobility), 25 times average cell throughput, and at least 10 times spectral and energy efficiency with five times lower latency. The main target of the 5G technology is to connect the entire world and to achieve extremely reliable, robust, and energy-efficient communication between anything (machine to machine, people to machine) or anybody (person to person) [1], [2]. Yet, the 5G technology is not completely standardized, and several research activities are performed on different technologies, work on different frequency bands in a range of frequencies between 5 and 70 GHz including the 28 GHz band [2], [3]. Furthermore, the 28 GHz band was among the highlighted bands above 24 GHz to be used for future mobile communications by the Federal Communications Commission [4]. Three-dimensional (3-D) printing, also known as additive manufacturing, is a promising technology that enables fast and cost-effective prototyping. Lately, several metal-plated, plastic 3-D-printed antennas have been reported, where the plastic prototypes are covered by metal through the conventional plating or metalization techniques [5]–[8].

In this letter, we propose two small, compact, efficient, and low-cost 3-D-printed antennas metalized using novel and simple techniques based on electromagnetic interference called as the radio frequency interference (EMI/RFI) conductive spray-paint technology. The proposed spray-coating technology is used to metalize the 3-D-printed plastic antenna instead of conventional metalization methods. The proposed metalization method reduces the cost of fabrication and reduces the complexity of the fabrication process.

II. Antenna Structure and Fabrication Method

The first proposed antenna (Ant-1) consists of a resonant slot surrounded by a rectangular cavity and two corrugations as shown in Fig. 1. The rectangular cavity and the two corrugations improve the directivity and gain of the antenna. In addition, the electromagnetic (EM) energy is coupled to the antenna surface using a standard rectangular waveguide by the means of resonant slot utilizing WR-28 (Ka-band) waveguide with dimensions $a \times b = 7.112$ mm $\times$ 3.556 mm. The waveguide length a is along the direction of slot length (SL), whereas the waveguide width is along the direction of slot width (SW). Hence, EM energy is coupled to the antenna surface along (SW) direction, which makes the electric field (E-field) polarized along the x-direction. The optimized dimensions that maximize the directivity of the antenna at resonance frequency can be summarized as follows:

$$W1 \approx L1 \approx \lambda \tag{1}$$

$$K \approx \frac{\lambda}{3} \tag{2}$$

$$D \approx \frac{\lambda}{5} \tag{3}$$

where λ is the resonance wavelength. The dimensions of the antenna are antenna length $L = 20$ mm, antenna width $W = 11$ mm, slot length SL $= 5.7$ mm, rectangular cavity length $L1 = 10.8$, plate thickness $T = 6.4$ mm, rectangular cavity width $W1 = 10.6$ mm, rectangular cavity depth $K = 3.2$ mm,

Manuscript received February 19, 2018; revised April 21, 2018 and May 27, 2018; accepted June 15, 2018. Date of publication June 19, 2018; date of current version October 26, 2018. This work was supported by the Physical Sciences Research Council (EPSRC) in the U.K. under Grant EP/R00711X/1. *(Corresponding author: Shaker Alkaraki.)*

S. Alkaraki, A. S. Andy, Y. Gao, R. Donnan, and C. Parini are with the School of Electronic Engineering and Computer Science, Queen Mary University of London, London E1 4NS, U.K. (e-mail: s.m.alkaraki@qmul.ac.uk; a.andy@qmul.ac.uk; yue.gao @qmul.ac.uk; r.donnan@qmul.ac.uk; c.g.parini@qmul.ac.uk).

K.-F. Tong is with the Department of Electronic and Electrical Engineering, University College London, London WC1E 7LE, U.K. (e-mail: k.tong@ucl.ac.uk).

Z. Ying is with Sony Mobile Communications, Lund 22188, Sweden (e-mail: ying.zhinong@sonymobile.com).

Digital Object Identifier 10.1109/LAWP.2018.2848912

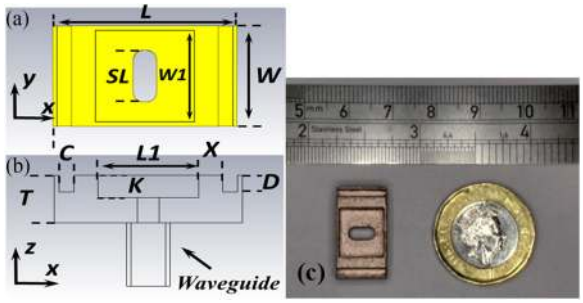

Fig. 1. Schematics of Ant-1. (a) Top view, (b) cross section of front view, and (c) fabricated prototype.

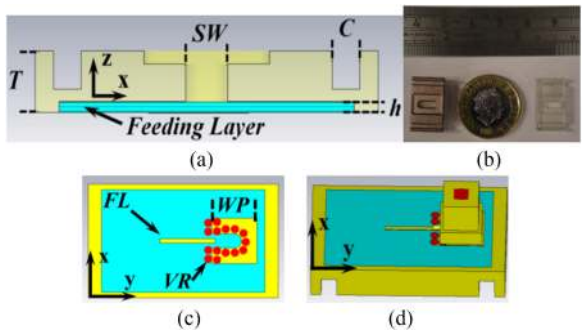

Fig. 2. Schematic of Ant-2. (a) Cross section of front view, (b) fabricated prototype, (c) bottom view, and (d) perspective bottom view with the connector. $W = 10$ mm, $T = 3$ mm, GW $= 1.5$ mm, $L = 17$ mm, $Gd = 1.9$ mm, $h = 0.508$ mm, $W1 = 9.5$ mm, $L1 = 7$ mm, $X = 3.2$ mm, SW $= 2.2$ mm, SL $= 6.5$ mm, FW $= 0.4$ mm, FL $= 5.4$ mm, VR $= 0.8$ mm, and WP $\times$ WP $= 4.4$ mm $\times$ 4.4 mm.

corrugation width $C = 1.6$ mm, corrugation depth $D = 2.1$ mm, and the distance between cavity and corrugation $X = 2.6$ mm. The proposed antenna is commonly fabricated using a metallic plate such as aluminium, and the corrugations and the slot are drilled using computer numerical control (CNC) milling and micromachining [7]. However, fabricating such a structure using CNC milling requires advanced machinery and skilled labor and produces a relatively heavy metallic prototype. Hence, to simplify the fabrication procedure, the antenna is 3-D printed in-house using a plastic material. The plastic material used is a transparent vero clear polyethylene, which enables fabrication of a solid, rigid, and light prototype with an overall weight of 1.35 g for Ant-1, which is $\sim$ 2–3 times lighter than an aluminum counterpart. A 3-D printer (Stratasys Objet30 Prime) is used to model the prototype as it prints with a layer thickness of 16 μm and a resolution of 100 μm. The prototype is 3-D printed with a clear finish, and the support material used in the 3-D printing process is effectively removed by rinsing the prototype using pressurized water. The cost of vero clear transparent polyethylene is $\approx$ \$650 USD per kg. Hence, the cost of material including the support material used to 3-D print the prototype is less than \$2 USD. Therefore, Objet30 offers cost-effective solutions to 3-D print small structures with high resolution for millimeter-wave applications. Then, the 3-D-printed plastic prototype is metalized using a commercial and low-cost conductive spray paint that has superior scratch resistance characteristics with very strong adhesive properties on a wide range of substrates [9]. This conductive metal spray consists of metallic particles and acrylic resin along with compressed air. Two coats of the conductive spray paint are applied directly to the surface of the antenna at room temperature with less than 1 h separation time between them. The paint typically dries within 5 min, and it delivers maximum conductivity after 24 h [9].

The schematic and the prototype of the second antenna (Ant-2) are shown in Fig. 2. Ant-2 is a smaller and a more compact version of Ant-1 due to a special microstrip feeding structure. Therefore, Ant-2 consists of two layers: The first layer is a feeding structure designed to feed the second layer, which is the 3-D-printed radiating structure. As shown in Fig. 2(c), the feeding layer is designed to accommodate the PE 44489 mini-surface mount package (SMP) connector. It consists of a transmission line, mini-SMP pad (ground plane), and vias fabricated on Rogers RO4003C substrate using conventional printed circuit board fabrication techniques to guarantee good performance. RO4003C is a hydrocarbon ceramic laminate, which has a dielectric constant of 3.38 and thickness of $h = 0.508$ mm. The second layer of Ant-2 is the radiating structure, and it is similar to Ant-1 as it contains a 3-D-printed resonant slot surrounded by a rectangular cavity and two corrugations. The commercial spray used for spray-coating is RS EMI/RFI 400 mL shielding aerosol available commercially at a cost of $\sim$\$50 USD per 400 mL can. Using the spray-coating technology to metalize the proposed 3-D-printed antenna over the conventional metalization techniques such as electroless plating has several advantages such as a significant cost reduction as metallizing Ant-1 and Ant-2 using the proposed technique costs less than \$2 USD for low-volume prototyping since the aerosol has a large coverage area of $\approx$1.25 square m per 400 mL [9]. Hence, the overall cost of fabrication of the antenna is very low if compared to CNC milling or if electroless plating is chosen as an alternative metalization technique. Furthermore, using spray coating simplifies the fabrication procedure since the paint can be used at room temperature, and the 3-D-printed prototypes do not need any special pretreatment or posttreatment process before or after spraying. In addition, the proposed spray-coating technique can be applied directly to open geometry structures such as Ant-1 and Ant-2, but it is not possible to be applied to complex and closed geometry structures unless they are disassembled as in [10]. One of the main disadvantages of the proposed metalization technique is that it is not possible to effectively control its thickness uniformity across the whole structure. Therefore, two coats were primarily applied to make sure that the interior sides of the slot and corrugations are painted, which makes the measured paint thickness on the surface of the prototype vary in the range of 45–65 μm, which is higher than the skin depth of copper $\sim$0.39 μm at 28.5 GHz. Hence, more expensive and complex plating techniques such as electroless plating [10] are recommended as a reliable alternative plating method, if the thickness of the metalization layer is highly critical.

III. Results and Analysis

A. Operating Principles

Ant-1 and Ant-2 share the same operating principles with a difference in the feeding method and the overall size, as Ant-2 has a smaller and a more compact size than Ant-1 with an overall thickness of 3 mm instead of 6.4 mm for Ant-1. For Ant-1 and Ant 2, the EM energy is coupled to the surface of the 3-D-printed structure via a resonant slot, where the resonance frequency of the slot is inversely proportional to its length (SL $\approx \frac{\lambda}{2}$), as shown in Fig. 3(a).

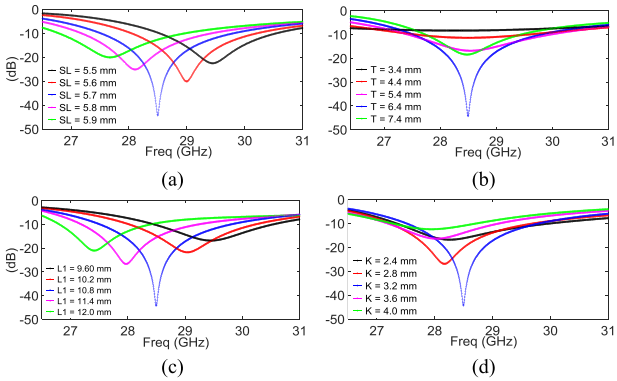

Fig. 3. Effect of Ant-1 parameters on S_{11}. (a) SL, (b) T, (c) $L1$, and (d) K.

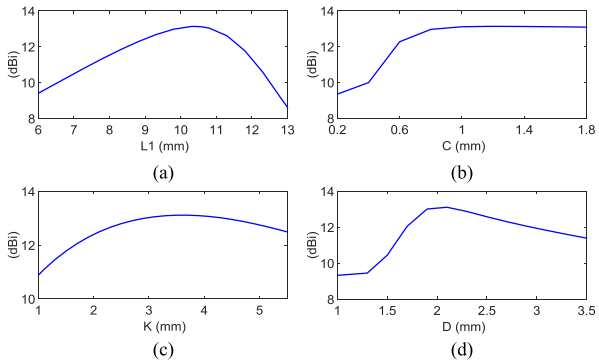

Fig. 4. Effect of Ant-1 parameters on the directivity. (a) $L1$, (b) C, (c) K, and (d) D.

The antennas offer high gain performance due to combined radiation from the slot, the rectangular cavity, and the corrugations. For instance, in Ant-1, the used WR28 waveguide operates in the dominant transverse electric (TE_{10}) mode, and it couples the EM energy to the surface of the antenna, where part of this energy is radiated by the slot, and the rest of the coupled energy is converted to a traveling wave that propagates in the x-direction on the surface of the antenna and ultimately lost and leaked at antenna edges. Hence, Ant-1 has a directivity of 5.6 dBi once the slot is solely present on the surface of the 3-D-printed structure, and this is due to conventional space-wave radiation from the slot. However, the directivity of the antenna is boosted by an extra ~3 dBi once the corrugations are added, and further by 4.4 dBi once the rectangular cavity is added. In fact, both the rectangular cavity and the corrugations excite the traveling wave on the surface of the antenna, resulting in an improvement in the directivity and gain performance of the antenna resulting in combined radiation in the boresight. Hence, the peak directivity performance is obtained once the dimensions of the cavity and the corrugations are optimized, as shown in Fig. 4. Moreover, the reason behind the gain improvement in the proposed antenna after the introduction of the rectangular cavity on the surface of the antenna is the radiation caused by the cavity due to strong excitation and resonance of the dominant (TM_{12}) mode inside the cavity, as shown in Fig. 5(b). Hence, the length of the cavity $L1$ has a major effect on the resonance frequency of the antenna, as shown in Fig. 3(c). Also, $L1$ has an effect on the directivity of the antenna as the peak in the directivity is obtained once $L1$ is equivalent to λ. Furthermore, the depth of the cavity K affects

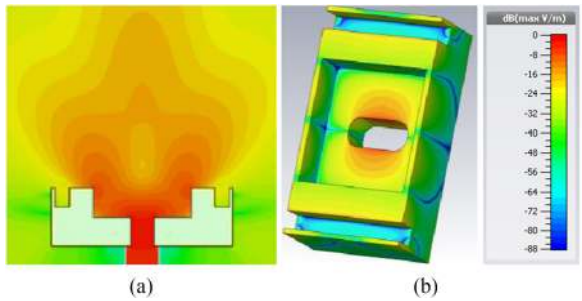

Fig. 5. Power flow for Ant-1 at (xz) cutting plane and E-field distribution on the surface of the antenna at 28.5 GHz. (a) Ant-1 power flow and (b) Ant-1 E-field.

the performance of the antenna, as shown in Figs. 3(d) and 4(c). For instance, the directivity sees a major improvement once K is larger than quarter-wavelength ($K = \frac{\lambda}{4} = 2.6$ mm) with a directivity of 12.7 dBi, and the maximum directivity of 13.2 dBi is obtained once K is in range of $\frac{3\lambda}{10} \leq K \leq \frac{4\lambda}{10}$, as shown in Fig. 4(c); hence, in the proposed design of Ant-1, K is set to $\frac{3\lambda}{10} = 3.2$ mm at 28.5 GHz. In addition, the two corrugations contribute to further ~ 3 dBi improvement in the directivity of the antenna due to excitation of the EM waves on the surface of the antenna, as analyzed in [11]–[15]. Furthermore, the main tradeoff of adding the cavity to the surface of Ant-1 with a depth of $K \approx \frac{\lambda}{3}$ is that the overall thickness of the antenna has to be increased. However, even with the cavity, Ant-1 is compact, and it has a superior aperture efficiency performance compared to the dimensions of other antennas with similar feeding structure such as PE 9850-15 standard horn or if compared to 5G antennas presented in [16] and [17].

B. Experimental and Numerical Results

Ant-1 and Ant-2 are numerically analyzed using CST Microwave Studio software, and the prototypes are fabricated and tested. Both structures were simulated as a perfect electric conductor (PEC) with an extremely smooth surface. The reflection coefficient is experimentally measured using a vector network analyzer, whereas the gain of the antennas has been measured using the standard horn gain comparison method described in detail in [18]. The measured results show that Ant-1 resonates at 28.5 GHz with a measured bandwidth of 2.5 GHz (8.8%) compared to a 2.3 GHz bandwidth in the simulation as shown in Fig. 6(a). The proposed antenna has a peak measured gain of 12.5 dBi at 28.7 GHz and a gain of 12.4 dBi at 28.5 GHz, as shown in Fig. 6(b), compared to a simulated gain of 13.2 dBi at 28.5 GHz. It is also observed, from Fig. 6(b), that the measured gain is more than 10 dBi over the entire bandwidth of the antenna, and the gain is particularly higher than 12 dBi over 800 MHz of the operating bandwidth. Besides, Ant-1 has a half-power beamwidth (HPBW) of 30° with sidelobe level of –12 dB in the E-plane and HPBW of 54° in the H-plane and with front-to-back (F/B) ratio of 20.1 dB.

In addition, one of the main figures of merit of Ant-1 is its compact size and high measured aperture efficiency (A_e). A_e is defined as the ratio of the maximum effective antenna aperture area to its physical aperture area, and it determines how efficiently the physical area of the antenna is utilized [19]. The outstanding A_e performance of Ant-1 is due to its high gain performance compared to its small size. Ant-1 has an A_e of 70%

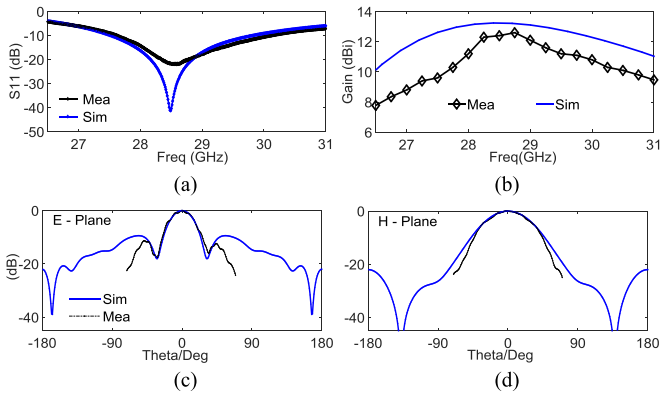

Fig. 6. Measured and simulated results of Ant-1. (a) S_{11}, (b) gain, (c) E-plane, and (d) H-plane at 28.5 GHz.

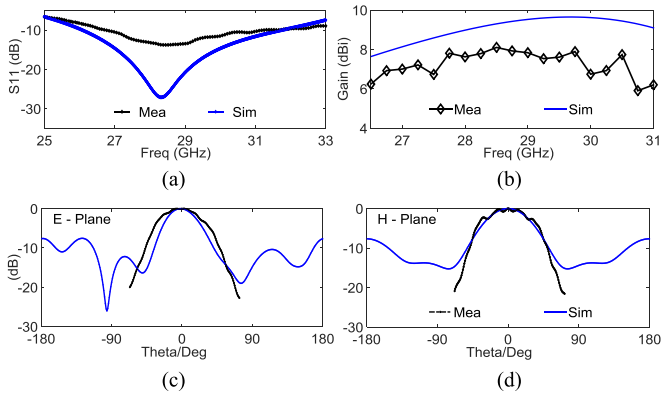

Fig. 8. Measured and simulated results of Ant-2. (a) S_{11}, (b) gain, (c) H-plane, and (d) E-plane at 28.5 GHz.

TABLE I
COMPARISON OF THE PROPOSED ANTENNAS PERFORMANCE WITH PE-HORN AND 5G ANTENNAS AT 28.5 GHZ

Antenna	Dimensions	Gain (dBi)	Bandwidth (%)	Ae (%)
Ant-1	$1.9\,\lambda \times 1.05\,\lambda \times 0.61\,\lambda$	12.4	8.8	70
Ant-2	$1.6\,\lambda \times 0.94\,\lambda \times 0.28\lambda$	8	12.9	33
Horn	$2.1\,\lambda \times 1.5\,\lambda \times 4.5\,\lambda$	13.5	≈ 40	59.5
[16]	$2.8\,\lambda \times 1.9\lambda \times 0.09\,\lambda$	7.5	≈ 8.7	8.3
[17]	$2.48\,\lambda \times 2\lambda \times 0.09\,\lambda$	12.7	≈ 20	30

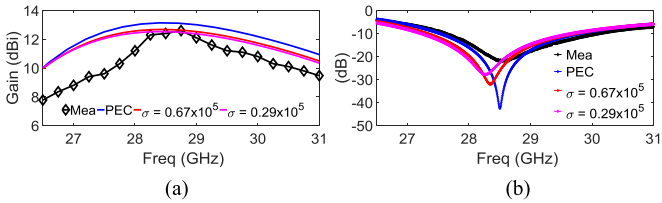

Fig. 7. Effect of conductivity on (a) the gain and (b) the S_{11} of Ant-1.

at 28.5 GHz, and A_e approaches a peak of 71.7% at 28.7 GHz. In comparison to an A_e of 59.5% for PE 9850-15 horn, 8.3% to the 28.5 GHz tilted beam 5G antenna fed by the waveguide and to an A_e of 30% at for 5G Franklin array has been presented recently in [17]. A detailed comparison between the proposed antennas performance with other antennas is shown in Table I. Furthermore, Ant-1 is compact once compared to the Ka-band PE 9850-15 horn as the horn is 7.4 times higher than Ant-1 with an overall height of 4.5λ at 28.5 GHz as compared to only 0.61λ in case of Ant-1. Generally, the measured gain of Ant-1 is in range of 0.7 to 2 dB lower than the simulated gain, as shown in Fig. 6(b), whereas the measured bandwidth is 200 MHz wider than the simulated one.

In fact, the lower gain and wider bandwidth are mainly due to the conduction losses introduced by the paint as shown in Fig. 7(a) and (b). The paint has a surface resistivity of $R_s = 0.3 - 0.7\,\Omega/\square$ at 50 μm thickness [9], which makes its conductivity $\sigma = 0.29 \times 10^5 - 0.67 \times 10^5$ S/m. This contributes to gain losses of 0.4$\sim$ 0.8 dB at 28.5 GHz compared to PEC as the simulation results show in Fig. 7(a). Hence, at 28.5 GHz, the antenna simulated gain is 13.2 dBi for PEC, 12.7 dBi for $\sigma = 0.67 \times 10^5$ S/m, and 12.5 dBi for $\sigma = 0.29 \times 10^5$ S/m, which is 0.1 dBi higher than the measured gain. Furthermore, fabrication tolerances and nonuniformity of the thickness of the paint might affect the S_{11} performance of the antenna as the paint thickness was not counted for in the simulation process, especially that the resonance frequency is sensitive to the dimensions of the slot as shown in Fig. 3(a). However, the surface roughness of the paint is hardly responsible for any gain losses. The measured root mean square (RMS) roughness of the paint at antenna surface is 4.92 μm along a path of 3 mm. However, it has been reported that a surface roughness of 25.9 μm (RMS) has no effect on the gain of a Ku-band horn antenna at 15 GHz, whereas a measured $\sim$ 0.7 dB loss in the horn gain is noticed once it has an extreme surface roughness of 39.7 μm (RMS), which is noticeably far larger than the proposed antenna surface roughness.

Furthermore, the measured and simulated reflection coefficient of Ant-2 is shown in Fig. 8(a), and it shows that the measured -10 dB bandwidth of the antenna is 3.7 GHz (12.9%) that ranges from 26.9 to 30.6 GHz. Furthermore, Ant-2 has a simulated peak gain of 9.6 dBi at 29.5 GHz and a simulated gain of 9.4 dBi at 28.5 GHz. However, the measured peak gain is 8 dBi at 28.5 GHz and 7.9 dBi at 29.5 GHz, and the antenna measured gain is higher than 7.6 dBi over 2 GHz bandwidth that ranges from 27.7 to 29.7 GHz, as shown in Fig. 8(b). The simulated and measured far-field radiation patterns of the antenna at 28.5 GHz are shown in Fig. 8. The proposed antenna has a measured HPBW of 60° in the H-plane and 53° in the E-plane, whereas the F/B ratio of the proposed antenna is 9.2 dB. The discrepancies between the simulated and measured results of Ant-2, besides the conduction losses as discussed in Ant-1 case, are due to insertion losses as well as matching losses due to mini-SMP connector soldering and misalignment with the 0.4 mm wide transmission line and fabrication tolerances of the feeding layer.

IV. CONCLUSION

This letter presents designs of efficient, high-gain, and compact 3-D-printed antennas metalized using low-cost EMI/RFI spray-coating technology. Using EMI/RFI conductive paint reduces the production cost of the antenna and the complexity of the fabrication procedure while delivering suitable performance at 28 GHz band. Finally, the novel fabrication method employed in this investigation offers the proposed antenna to be a potential candidate for low-cost 5G mm-wave applications.

REFERENCES

[1] Ericsson.com, "Mobility report," 2015. [Online]. Available: http://www.ericsson.com/res/docs/2015/ericsson-mobility-report-june-2015.pdf. Accessed: Jan. 5, 2018.

[2] NTT Docomo Inc., "NTT DOCOMO's views on 5G," 2014. [Online]. Available: http://johannesbergsummit.com/wp-content/uploads/sites/6/2013/11/Nakamura-Johnnesberg-Summit-NTT-DOCOMOs-Views-on-5G_rev.pdf. Accessed: Jan. 5, 2018.

[3] S. F. Jilani and A. Alomainy, "Millimetre-wave T-shaped MIMO antenna with defected ground structures for 5G cellular networks," *Microw., Antennas Propag.*, vol. 12, no. 5, pp. 672–677, 2018.

[4] FCC, "Use of Spectrum Bands above 24 GHz for Mobile Radio Services, GN Docket No. 14-177, Notice of Proposed Rulemaking," 15 FCC Record 138A1. Oct. 23, 2015.

[5] G. P. Le Sage, "3D printed waveguide slot array antennas," *IEEE Access*, vol. 4, pp. 1258–1265, 2016.

[6] J. A. Gordon *et al.*, "An all-metal, 3-D-printed CubeSat feed horn: An assessment of performance conducted at 118.7503 GHz using a robotic antenna range," *IEEE Antennas Propag. Mag.*, vol. 59, no. 2, pp. 96–102, Apr. 2017.

[7] U. Beaskoetxea, S. Maci, M. Navarro-Cía, and M. Beruete, "3-D-printed 96 GHz bull's-eye antenna with off-axis beaming," *IEEE Trans. Antennas Propag.*, vol. 65, no. 1, pp. 17–25, Jan. 2017.

[8] Y. Tawk, M. Chahoud, M. Fadous, J. Costantine, and C. G. Christodoulou, "The miniaturization of a partially 3D printed quadrifilar helix antenna," *IEEE Trans. Antennas Propag.*, vol. 65, no. 10, pp. 5043–5051, Oct. 2017.

[9] RS EMI/RFI Shielding Aerosol with Bronze colour 400mL data Sheet. [Online]. Available: https://docs-emea.rs-online.com/webdocs/1583/0900766b8158361e.pdf. Accessed: Apr. 20, 2018.

[10] M. D'Auria *et al.*, "3-D printed metal-pipe rectangular waveguides," *IEEE Trans. Compon., Packag. Manuf., Technol.*, vol. 5, no. 9, pp. 1339–1349, Sep. 2015.

[11] S. Alkaraki, Y. Gao, and C. Parini, "High aperture efficient antenna at Ku band," in *Proc. Int. Workshop Electromagn.: Appl. Student Innov. Competition*, London, U.K., 2017, pp. 60–62.

[12] D. Y. Na, K. Y. Jung, and Y. B. Park, "Transmission through an annular aperture surrounded with corrugations in a PEC plane," *IEEE Antennas Wireless Propag. Lett.*, vol. 14, pp. 179–182, 2015.

[13] S. Alkaraki, Y. Gao, and C. Parini, "Dual-layer corrugated plate antenna," *IEEE Antennas Wireless Propag. Lett.*, vol. 16, pp. 2086–2089, 2017.

[14] M. B. Diaz *et al.*, "Dual-band low-profile corrugated feeder antenna," *IEEE Trans. Antennas Propag.*, vol. 54, no. 2, pp. 340–350, Feb. 2006.

[15] S. Alkaraki, Y. Gao, and C. Parini, "Small and high gain millimetre wave corrugated grooves antenna," in *Proc. IEEE Int. Symp. Antennas Propag. USNC/URSI Nat. Radio Sci. Meeting*, Vancouver, BC, Canada, 2015, pp. 2091–2092.

[16] J. S. Park, J. B. Ko, H. K. Kwon, B. S. Kang, B. Park, and D. Kim, "A tilted combined beam antenna for 5G communications using a 28-GHz Band," *IEEE Antennas Wireless Propag. Lett.*, vol. 15, pp. 1685–1688, 2016.

[17] S. F. Jilani and A. Alomainy, "A multiband millimeter-wave 2-D array based on enhanced franklin antenna for 5G wireless systems," *IEEE Antennas Wireless Propag. Lett.*, vol. 16, pp. 2983–2986, 2017.

[18] C. A. Balanis," Antenna measurement," in *Antenna Theory*, 3rd ed. Hoboken, NJ, USA: Wiley, 2005, ch. 17, sec. 4.2, pp. 1033–1034.

[19] C. A. Balanis, "Aperture antennas," in *Antenna Theory*, 3rd ed. Hoboken, NJ, USA: Wiley, 2005, ch. 12, sec. 5.3, p. 682.